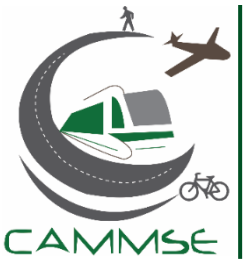

Center for Advanced Multimodal Mobility Solutions and Education

Project ID: 2018 Project 08

ASSESSMENT OF PARCEL DELIVERY SYSTEMS USING UNMANNED AERIAL VEHICLES

Interim Report

by

Stephen D. Boyles, Ph.D. (ORCID: https://orcid.org/0000-0002-5414-5438)
Associate Professor, Department of Civil and Environmental Engineering
Consortium Member
301 E Dean Keeton St. Stop C1761, Austin, TX 78712-1172
Phone: 1-512-471-3548; Email: sboyles@mail.utexas.edu

Cesar Yahia, M.S. (ORCID: https://orcid.org/0000-0001-9062-8149)
Graduate Research Assistant, Department of Civil and Environmental Engineering
Consortium Member
301 E Dean Keeton St. Stop C1761, Austin, TX 78712-1172
Phone: 1-512-471-3548; Email: cesaryahia@utexas.edu

for

Center for Advanced Multimodal Mobility Solutions and Education
(CAMMSE @ UNC Charlotte)
The University of North Carolina at Charlotte
9201 University City Blvd
Charlotte, NC 28223

September 2019

ACKNOWLEDGEMENTS

This project was funded by the Center for Advanced Multimodal Mobility Solutions and Education (CAMMSE @ UNC Charlotte), one of the Tier I University Transportation Centers that were selected in this nationwide competition, by the Office of the Assistant Secretary for Research and Technology (OST-R), U.S. Department of Transportation (US DOT), under the FAST Act. The authors are also very grateful for all of the time and effort spent by DOT and industry professionals to provide project information that was critical for the successful completion of this study.

DISCLAIMER

Table of Contents

List of Figures

EXECUTIVE SUMMARY

Unmanned aerial vehicles (drones) can be used in traffic and road monitoring applications. We investigate methods for routing a drone that is capable of simultaneously detecting road conditions and estimating traffic densities. First, we analyze the impact of incidents on model parameters and the difficulty in detecting capacity drops under congested conditions using speed-density observations. Then, we propose a framework for adaptively navigating a drone to minimize the uncertainty on parameter and traffic state estimates. This framework (1) assimilates drone observations and local sensor data, (2) quantifies the uncertainty on road network conditions and traffic states, and (3) navigates the drone towards targeted observations that minimize this uncertainty. Compared to estimation without a drone, we show that we can obtain significant improvement in traffic estimation and incident detection by adaptively navigating a mobile sensor that is capable of detecting capacity drops. In the future, the proposed drone navigation framework will be used for evaluating the benefit of parcel delivery systems that rely on drone detection and delivery capabilities.

Chapter 1. Introduction

1.1 Problem Statement

Non-recurrent congestion is caused by capacity reducing incidents such as accidents, adverse weather conditions, and work zones. This type of congestion is considered to be the primary source of travel time variability and accounts for up to 30% of congestion delay during peak periods [1, 2]. Traditionally, nonrecurrent congestion detection methods rely on comparing expected traffic conditions with sensor measurements. These algorithms detect that an incident occurred once collected data significantly deviates from expected conditions [3]. However, such outlier-based methods suffer from random traffic fluctuations that cause false alarms, and they are not capable of distinguishing incident data from traffic patterns that occur due to shock waves [3, 4].

Furthermore, to improve traffic state estimates under non-recurrent congestion, incident information should be integrated into traffic models by modifying certain parameters that reflect incident severity [5]. This led researchers to explore model-based traffic estimation methods for jointly estimating the traffic state and parameters pertaining to incidents [6, 7]. Recent estimation techniques rely on comparing traffic model predictions with observed data to identify the most likely parameter among a set of model parameters that correspond to different levels of incident severity [5, 8, 9, 10]. These methods are promising but they are still limited in certain situations where it is difficult to determine if observed speed-density measurements corresponds to congestion under normal operating conditions or an actual reduction in road capacity.

In this project, we aim to develop a framework that navigates a drone for simultaneously estimating traffic states and road network condition. The proposed drone routing algorithm seeks to minimize the uncertainty on the network conditions. This results in informative drone observations that supplement data collected from ground sensors. The observations collected by the drone and ground sensors can be subsequently used in algorithms that require real-time traffic data. For example, novel drone-assisted parcel delivery algorithms can exploit this information to determine optimal truck tours and drone deployment strategies.

1.2 Objectives

We propose a coupled estimation and planning framework that exploits the capability of mobile unmanned aerial vehicles (drones) in detecting road and traffic conditions. In particular, this framework (1) assimilates drone density and capacity drop observations with local speed-density sensor measurements (2) quantifies the uncertainty on road and traffic states, and (3) adaptively navigates the drone towards uncertainty minimizing road and traffic state observations. We note that the proposed routing framework can be used to navigate a mobile sensor towards traffic state uncertainty minimizing observations without updating parameters that represent incident severity. Similarly, the estimation framework can be used to quantify the relative uncertainty on traffic states and parameters without using targeted drone observations to minimize this uncertainty. While previous studies evaluated the benefit of using incident information to adjust model parameters and obtain improved traffic state estimates [5, 6, 8, 9, 10, 11, 12], we

show that generating targeted uncertainty minimizing observations using a drone further improves both state and parameter estimates. The proposed framework is shown in Figure 1.

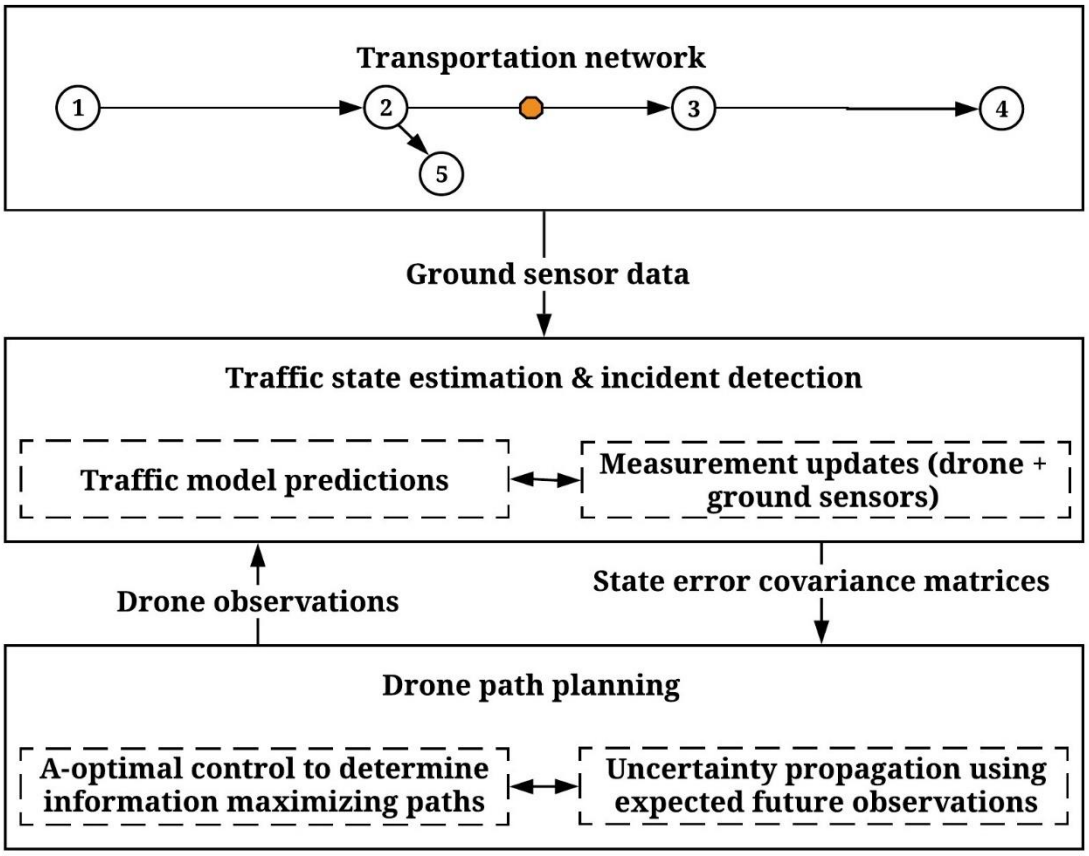

Figure 1 Estimation and routing framework to navigate a drone towards informative traffic state and incident observations.

1.3 Expected Contributions

Thus, the main contributions include:

1- An algorithm for routing drones to maximize information on the traffic and road network state
2- Quantification of the uncertainty on the road network state relative to the corresponding uncertainty on the traffic state
3- A framework for integration of information from ground sensors and drone observations to estimate traffic characteristics and road conditions

1.4 Report Overview

The remainder of this report is organized as follows. Chapter 2 discusses the literature relevant to incident detection and traffic state estimation. In Chapter 3, we analyze the impact of non-recurrent congestion on traffic model parameters and present a dual ensemble Kalman filter (EnKF) algorithm for simultaneous state and parameter estimation. Then, we discuss the difficulty in estimating capacity drops from speed-density measurements, we quantify the uncertainty on the dual EnKF estimates, and we develop the framework shown in Figure 1 to incorporate uncertainty minimizing drone observations into the estimation procedure. In Chapter 4, we present results obtained for a simulated freeway segment that show the advantage of generating targeted observations in congested conditions. This chapter also discusses conclusions and future work.

Chapter 2. Literature Review

2.1 Data-Driven Incident Detection

The majority of incident detection methods rely on evaluating abnormalities in observed traffic data [3]. Data-driven methods include threshold-based algorithms that have been applied since the 1970's. These threshold-based algorithms compare patterns from detector observations to threshold values in a decision tree [13]. Subsequently, alternative data-driven approaches such as time series analysis, artificial neural networks, and wavelet-based techniques have been used to detect traffic incidents [3, 4, 14, 15, 16]. Comprehensive reviews on such incident detection algorithms can be found in [17, 18]. The primary drawbacks of data-driven methods pertain to (1) fitting or specifying a large number of parameters, (2) difficulty in distinguishing between traffic patterns from incidents and similar data due to congestion under normal operating conditions, (3) susceptibility to random fluctuations in traffic data, and (4) difficulty in adequately predict traffic states due to the lack of a model representing traffic flow dynamics [10, 17, 18].

2.2 Incident Detection and Traffic Estimation

To detect incidents and predict the corresponding traffic dynamics, researchers explored model-based estimation methods that simultaneously estimate traffic states and parameters that reflect incident severity. Wang and Papageorgiou [7] proposed an extended Kalman filter that uses a macroscopic traffic flow model to estimate densities as well as calibrate the free flow speed and critical density. They implemented joint state estimation in which parameters and boundary variables are added to the state space, and they considered that flow and mean speed measurements could be obtained. Recent articles on simultaneous estimation of states and fundamental diagram parameters include the use of count and trajectory data in a single optimization framework [19], and a moving horizon approach that determines the traffic state and incident parameters which minimize a quadratic cost function [6].

Alternative model-based estimation techniques include methods that aim to identify the most likely traffic model given observed data. In the case of incident detection, each traffic model represents a different parametrization that reflects a certain level of incident severity. The first article to consider this approach used an extended Kalman filter to select the most likely model [8]. Then, this framework was enhanced to allow for dependencies between the most likely traffic models chosen across time steps [5]. Specifically, an interactive multiple model ensemble Kalman filter and a multiple model particle filter were developed to simultaneously estimate traffic state and incident severity given specified incident evolution dynamics [5, 9, 10].

For typical sensor data such as speed and occupancy measurements, the aforementioned model-based estimation methods are not able to distinguish between congestion observations due to incidents and similar observations from congested states under normal operating conditions. This difficulty to detect capacity drops will be analyzed in Chapter 3.

To address this problem of detecting the underlying road network condition, we propose the use of unmanned aerial vehicles that are capable of detecting capacity drops by analyzing road

network imagery. In addition, the drones can collect traffic speed and density observations as they traverse the network by analyzing objects in a frame across time [21, 22].

Thus, the objective of this project is to develop a framework for simultaneous traffic parameter-state estimation and drone navigation. In addition to drone observations, we assume that density data from loop detectors and less frequent speed measurements from GPS equipped probe vehicles are available. For estimation, we use a dual state-parameter ensemble Kalman filter (EnKF) with traffic dynamics represented by the cell transmission model (CTM). This generates time varying Gaussian distributions that represent the uncertainty on parameter and state estimates. Then, to minimize this uncertainty, we develop an online one-step lookahead path planning algorithm that evaluates candidate drone trajectories based on anticipated reduction in average variance of state and parameter estimates.

Chapter 3. Solution Methodology

3.1 Introduction

This Chapter present the estimation and planning framework shown in Figure 1. First, we analyze the impact of incidents on traffic model parameters. Then, we develop a dual state ensemble Kalman filter algorithm for simultaneously estimating traffic states and model parameters. We show that estimation using the aforementioned algorithm is limited in congested conditions where it is difficult to distinguish speed-density observations due to a reduction in capacity from similar observations due to congestion under normal operating conditions. Thus, we develop a modified estimation algorithm that (1) quantifies the relative uncertainty on traffic states and incident condition and (2) navigates a drone towards observations that maximize the information state.

3.2 Traffic State and Parameter Estimation under Non-Recurrent Congestion

In this section, we analyze the impact of incidents on parameters of the cell transmission model which is used to represent traffic dynamics. The analysis will be used in Chapter 3.3 to determine how model parameters should be updated based on observed data by considering the non-linearities involved in representing traffic dynamics.

Non-Recurrent Congestion Impact on Traffic Model Parameters

The Lighthill-Whitham-Richards partial differential equation (LWR PDE) is used to represent traffic dynamics. This is shown in Equation 1 where $\rho(x,t)$ and $v(\rho(x,t))$ are the density and velocity at a particular point in space and time, respectively. We use a speed-density relationship defined in Equation 2 that corresponds to a triangular flow-density diagram. In this equation, ρ_{cr} is the critical density, ρ_j is the jam density, and v_{max} is the free flow speed.

$$\frac{\partial \rho(x,t)}{\partial t} + \frac{\partial (\rho(x,t) v(\rho(x,t)))}{\partial x} = 0 \tag{1}$$

$$v(\rho(x,t)) = \begin{cases} v_{max} & \text{for } \rho(x,t) \leq \rho_{cr} \\ \frac{v_{max}\rho_{cr}(\rho_j - \rho(x,t))}{\rho(x,t)(\rho_j - \rho_{cr})} & \text{otherwise} \end{cases} \tag{2}$$

The LWR PDE is discretized for practical implementation using a Godunov scheme to obtain the cell transmission model (CTM) [24, 25, 26]. Specifically, time is discretized into time steps of duration Δt, and space is discretized into cells of length Δx such that $\Delta x = v_{max}\Delta t$. Letting $n(x,t)$ be the number of vehicles in cell x at time t and $y(x,t)$ be the number of vehicles entering cell x at the t-th time step, we can approximate $n(x,t)$ and $y(x,t)$ using Equations 3 and 4. Then, we can determine $y(x,t)$ using Equation 5 and $n(x,t)$ using Equation 6. The calculated $n(x,t)$ values can be used to track densities in cells across time via Equation 3.

$$n(x,t) \approx \rho(x,t)\Delta x \tag{3}$$

$$y(x,t) \approx \rho(x,t)v(\rho(x,t))\Delta t \tag{4}$$

$$y(x,t) = \min\left\{ n(x-\Delta x,t), \frac{\rho_{cr}}{\rho_j - \rho_{cr}}\left(\rho_j \Delta x - n(x,t)\right)\right\} \tag{5}$$

$$n(x,t+\Delta t) = n(x,t) + y(x,t) - y(x+\Delta x,t) \tag{6}$$

To investigate the impact of non-recurrent congestion on the speed-density relationship and vehicle throughput, we use the PTV VISSIM microsimulation software with reduced speed zones representing non-recurrent congestion regions [27]. Note that the non-recurrent congestion incidents we consider do not significantly impact the jam density. This type of incidents could represent adverse weather conditions or roadside accidents and work zones. Compared to existing methods that determine the change in parameters for lane-blocking incidents using Highway Capacity Manual (HCM) recommendations and a fixed incident free flow speed [5, 9, 10], we aim to develop a relationship that determines the change in critical density as a function of reductions in free flow speed.

First, we calibrate the speed-density relationship without any incidents for a three-lane freeway by fitting Equation 2 through data points generated at a particular location along the freeway. The dashed line in Figure 2 corresponds to the fitted relationship under normal operating conditions. Then, we introduce different levels of incident severity using reduced speed zones and determine a least-squares fit for a piecewise linear function through the observed speed and density data points. The intersection point of the line segments indicates the critical density corresponding to a particular incident free flow speed. As shown in Figure 2, the critical density increases with reduced speed. This is expected since at lower free flow speeds, vehicles can travel with shorter headways before backward shock waves are initiated. The observed relationship will guide parameter updates in the estimation procedure that will be discussed next.

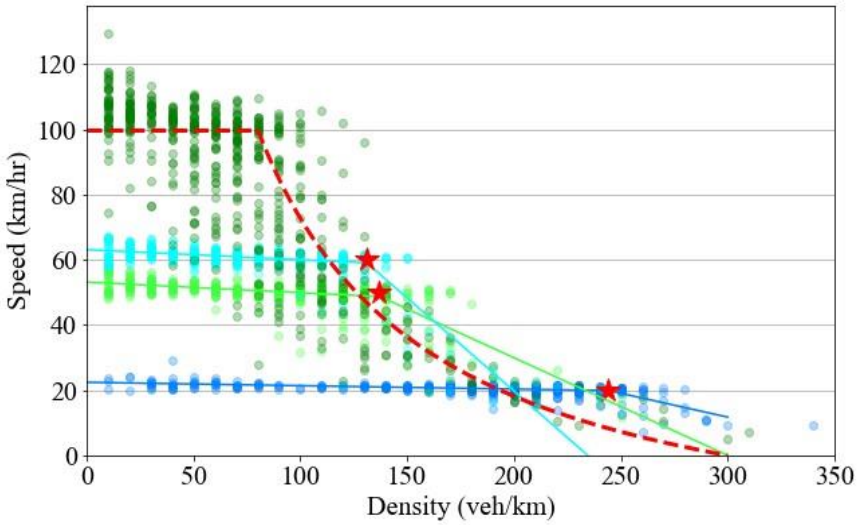

Figure 2 Impact of non-recurrent congestion on the speed-density relationship. Star markers indicate change in critical density resulting from the corresponding reduction in free flow speed.

3.3 Dual State Ensemble Kalman Filter

We use a dual state space ensemble Kalman filter (EnKF) to estimate traffic state and incident severity across time [28, 29, 30]. The traffic state is represented by densities propagated forward using the cell transmission model with additive Gaussian white noise. The incident severity is represented by the free flow speed parameters v_{max} at incident prone locations. These parameters are propagated forward using a random walk. In terms of observations, the traffic state is directly observed using loop detector density measurements while the incident parameter v_{max} is observed using Equation 2 given less frequent speed measurements.

The dual state EnKF is composed of two separate ensemble Kalman filters for traffic states and free flow speed working in parallel. Each EnKF is a stochastic filter that propagates ensemble members (samples) representing the state statistics. The filters interact by recursively feeding best estimates into each other at every update step. In particular, the updated parameters are used to adjust the forward model of the traffic state EnKF, and the resulting traffic state estimates inform subsequent parameter updates. In each filter, the ensemble mean is the best estimate on the true traffic state/parameter and the ensemble covariance corresponds to the error on the ensemble mean [28, 29].

While alternative optimization methods could be used to freely specify the estimation objectives [23], the dual EnKF is a variance minimizing scheme that enables efficient updating of Gaussian covariance matrices which we exploit for drone path planning. In addition, compared to methods that estimate the most likely traffic model [5, 8, 9, 10], the dual EnKF uses continuous incident parameters and is thus not limited to a specified set of incident severity levels. Dual

estimation procedures are not capable of capturing correlation between the parameters and traffic state variables since they maintain separate filters. However, estimation of parameters based on filtered state estimates may result in smoother parameter estimates [31, 32, 33].

Importantly, the dual estimation procedure allows for integration of data at different time scales to update v_{max} parameters only when speed measurements are collected. Furthermore, using a dual state estimation procedure allows us to maintain separate covariance matrices for states and parameters. Maintaining separate covariance matrices is a critical component of the proposed drone navigation algorithm (Section 4) that aims to identify targeted uncertainty minimizing drone measurements.

Traffic State EnKF

The traffic state EnKF is shown in Equations 7–14 where $\mathbf{k}_j^t$ is a vector of densities corresponding to ensemble member j at time t [28]. $\text{CTM}_{\Delta t}$ represents forward propagation of densities from time t until time $t + \Delta t$ using Equations 3– 6, and w is Gaussian noise that reflects model errors. For N ensemble members, $\mathbf{A}$ is a matrix in which the columns are the ensemble members, $\mathbf{1}_N$ is an $N \times N$ scale matrix such that every element is $1/N$, and $\bar{\mathbf{A}}$ is a matrix where every column is the ensemble mean.

In terms of observations, $\mathbf{d}_j$ represents a particular perturbation of the density measurements d using Gaussian observation errors denoted as ε, and $\mathbf{D}$ is a matrix storing the perturbed observations. Υ is a matrix storing the observation perturbations. In addition, $\mathbf{H}$ is an observation matrix which in this case is the identity matrix since state density variables are observed directly.

The updated ensemble members $\mathbf{k}_j^{t+\Delta t}$ are stored in columns of matrix $\mathbf{A}^a$ and $\mathbf{P}$ is the updated ensemble covariance matrix. This analysis procedure is a variance minimizing scheme that enables nonlinear propagation of error statistics and iteratively computes the best state estimates. Compared to the extended Kalman filter, this procedure does not require linearizations and efficiently propagates the state error covariance matrix using ensemble members [28].

$$\mathbf{k}_j^{t+\Delta t|t} = \mathrm{CTM}_{\Delta t}[\mathbf{k}_j^t] + w \quad \forall j \in \{1,..,N\} \tag{7}$$

$$\mathbf{A} = (\mathbf{k}_1^{t+\Delta t|t}, \mathbf{k}_2^{t+\Delta t|t}, ..., \mathbf{k}_N^{t+\Delta t|t}) \tag{8}$$

$$\bar{\mathbf{A}} = \mathbf{A}\mathbf{1}_\mathbf{N} \tag{9}$$

$$\mathbf{d_j} = \mathbf{d} + \varepsilon_j \quad \forall j \in \{1,..,N\} \tag{10}$$

$$\mathbf{D} = (\mathbf{d_1}, \mathbf{d_2}, ..., \mathbf{d_N}) \tag{11}$$

$$\Upsilon = (\varepsilon_1, \varepsilon_2, ..., \varepsilon_N) \tag{12}$$

$$\mathbf{A^a} = \mathbf{A} + (\mathbf{A} - \bar{\mathbf{A}})(\mathbf{A} - \bar{\mathbf{A}})^T\mathbf{H}^T(\mathbf{H}(\mathbf{A} - \bar{\mathbf{A}})(\mathbf{A} - \bar{\mathbf{A}})^T\mathbf{H}^T + \Upsilon\Upsilon^T)^{-1}(\mathbf{D} - \mathbf{HA}) \tag{13}$$

$$\mathbf{P} = \frac{1}{N-1}(\mathbf{A^a} - \mathbf{A^a}\mathbf{1_N})(\mathbf{A^a} - \mathbf{A^a}\mathbf{1_N})^T \tag{14}$$

Free Flow Speeds EnKF

The ensemble Kalman filter for estimating the free flow speeds at incident prone locations vmax follows a similar procedure to the densities EnKF. The parameters are propagated through a random walk as shown in Equation 15 where vtj is an ensemble member containing the free flow speeds at incident prone locations. The random walk reflects the change in incident severity across time where z is Gaussian noise.

$$\mathbf{v}_j^{t+\Delta t|t} = \mathbf{v}_j^t + z \tag{15}$$

The primary difference between the traffic state EnKF and free flow speed EnKF is the nonlinear observation operator. Specifically, if we consider that the critical density ρ_{cr} is a function of the free flow speed v_{max} as shown in Figure 2, then it would not be possible to create the linear observation matrix H. If we ignore the dependence of ρ_{cr} on v_{max}, we can construct time varying observation matrices that correspond to the observed velocities using Equation 2 (given assimilated densities from the traffic state EnKF). However, this leads to a poor performance of the filter.

To incorporate nonlinear observations, we introduce diagnostic variables that represent model predicted measurements into the state space [29]. In particular, we introduce the matrix $\widehat{\mathbf{A}}$ such that its columns are predicted velocities computed through a nonlinear function, $\mathrm{M}(\cdot)$, which represents Equation 2 and accounts for the dependence of ρ_{cr} on v_{max}. $\widehat{\mathbf{A}}$ is defined in Equation 16. Subsequently, the ensemble update equation is replaced with Equation 17 which essentially relates the model predicted velocity measurements (velocity that should be observed given v_{max}) to the actual collected velocity measurements and accordingly updates the v_{max} estimates.

$$\hat{\mathbf{A}} = (\mathsf{M}(\mathbf{v}_1^{t+\Delta t|t}), \mathsf{M}(\mathbf{v}_2^{t+\Delta t|t}), ..., \mathsf{M}(\mathbf{v}_N^{t+\Delta t|t})) \quad (16)$$

$$\mathbf{A^a} = \mathbf{A} + (\mathbf{A} - \bar{\mathbf{A}})(\hat{\mathbf{A}} - \hat{\mathbf{A}}\mathbf{1_N})^T((\hat{\mathbf{A}} - \hat{\mathbf{A}}\mathbf{1_N})(\hat{\mathbf{A}} - \hat{\mathbf{A}}\mathbf{1_N})^T + \Upsilon\Upsilon^T)^{-1}(\mathbf{D} - \hat{\mathbf{A}}) \quad (17)$$

Dual EnKF Parameter Update Procedure

After updating the densities using the traffic states EnKF and v_{max} using the free flow speed EnKF, we need to update ρ_{cr} to account for the increase in critical density as a function of reduced speed (Section 3.1). This ρ_{cr} update is limited by the non-linearity of the observations in the free flow speed EnKF. In particular, the procedure for introducing diagnostic variables to address nonlinearities works well in situations where the function $\mathsf{M}(\cdot)$ is monotonic and not highly nonlinear [29]. If $\mathsf{M}(\cdot)$ is non-monotonic, then it would not be clear if the free flow speed EnKF should increase or decrease v_{max} with a change in observed speed.

To maintain monotonic $\mathsf{M}(\cdot)$ functions, we consider that as v_{max} varies, the backward wave speed remains fixed at the calibrated value in incident free conditions. Graphically, this corresponds to updating the fundamental diagrams as shown using dashed lines in Figure 3. The updated critical density $\rho_{cr}{}^t$ for any value $v^t{}_{max}$ is then given by Equation 18 where $v^0{}_{max}$ and $\rho_{cr}{}^0$ are the original calibrated parameters under incident-free conditions. From Figure 2, we assume that the star markers will lie on the dashed line, which we believe is a reasonable assumption.

We note that if ρ_{cr} and v_{max} are otherwise updated such that at any stage the backward wave speed increases when v_{max} decreases or vice versa, the resulting $\mathsf{M}(\cdot)$ functions will be non-monotonic. Physically, an inverse correlation between the backward wave speed and v_{max} implies that within a certain high-density region we are capable of sending greater flow at a lower free flow speed. Thus, in addition to creating non-monotonic $\mathsf{M}(\cdot)$ functions, an inverse correlation between backward wave speed and v_{max} would not be representative of actual traffic dynamics.

$$\rho_{cr}^t = \frac{\rho_{cr}^0 v_{max}^0 \rho_j}{v_{max}^t(\rho_j - \rho_{cr}^0) + \rho_{cr}^0 v_{max}^0} \quad (18)$$

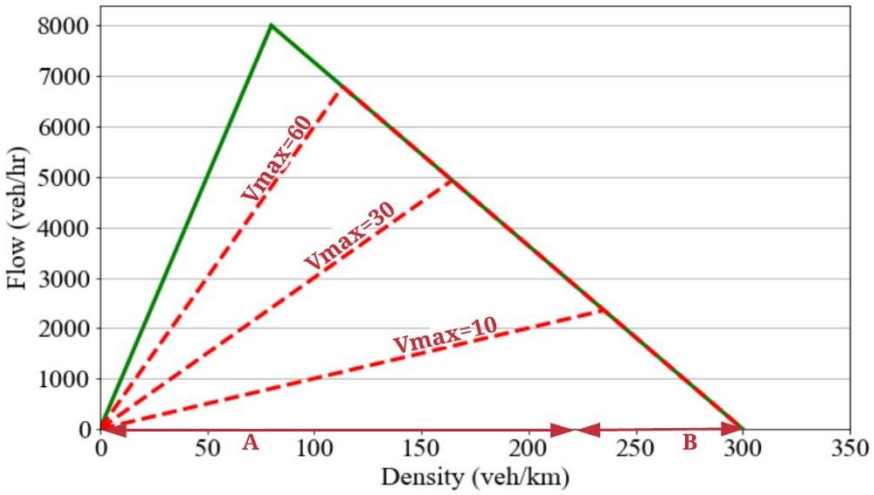

Figure 3 Change in fundamental diagram with increasing incident severity. Dashed lines correspond to incident fundamental diagram.

The Dual State EnKF Algorithm

Therefore, in the dual EnKF estimation procedure, we iteratively update traffic state estimates using Equations 7–14. Once we observe speed measurements, we use the ensemble mean of the assimilated densities for updating the free flow speed parameters via an EnKF approach for handling nonlinear observations by introducing diagnostic variables. Then, the ensemble mean of the v_{max} EnKF is used to update the parameters v_{max} and ρ_{cr} in the $CTM_{\Delta t}$ forward model until future velocity measurements are obtained. Thus, the filters recursively feed best estimates into each other while updating the traffic state and the model incident parameter. This dual EnKF procedure is shown in Algorithm 1.

Algorithm 1 Dual EnKF for traffic states and free flow speed parameters at incident prone locations

Initialization:

(1) Define $\mathrm{CTM}_{\Delta t}$ based on incident-free calibrated parameters
(2) Create initial ensembles for densities across cells
(3) Create initial ensembles for free flow speeds at incident prone locations

Dual EnKF:

for *time* in *estimation horizon* **do**
  (4) Propagate density ensembles forward using Equations 3–6
  (5) Update ensembles using densities EnKF through Equations 7–14
  if get speed observation **then**
    (6) Propagate free flow speeds ensembles using Equation 15
    (7) Use mean of densities ensemble, Equations 2, 7–12, and 14–18 to update ensembles via free flow speeds EnKF
    (8) Update v_{max} and ρ_{cr} parameters in $\mathrm{CTM}_{\Delta t}$ using mean of free flow speeds EnKF and Equation 18

3.4 Drone Navigation for Uncertainty Minimization and Traffic State-Parameter Estimation

The proposed dual state estimation procedure in Section 3 can efficiently estimate states and parameters in situations where the densities vary significantly during the estimation time horizon. In addition, given low values of density as shown in region A of Figure 3, we can effectively distinguish between speed observations that we expect the different fundamental diagrams to generate.

However, in region B of Figure 3, the fundamental diagrams coincide and they are difficult to distinguish from speed and density observations. This is expected in any estimation procedure that attempts to estimate the free flow speed or capacity from speed and density observations. Given high densities and low speed measurements, we would not be able to determine whether the observations correspond to congested conditions in an incident-free fundamental diagram or if there is a reduction in physical capacity and free flow speed. In terms of the dual EnKF method, this would result in a high variance on the parameter estimates.

To address this estimation problem in region B, we propose the use of unmanned aerial vehicles to directly estimate incident severity and traffic state. Drones can be equipped with cameras to monitor road and traffic conditions [20]. Then, by analyzing objects in a frame across time they can detect capacity drops and collect speed-density measurements [21, 22]. In particular, we consider that the drone can collect accurate speed-density measurements as well as direct v_{max} observations up to observation errors.

In this section, we develop a drone navigation framework such that the drone moves along paths that minimize the anticipated future variance on dual EnKF state errors. To minimize

this variance in an online setting where the state covariance matrices are continuously updated, we develop a one-step lookahead path planning algorithm.

A-optimal Control Trajectory Planning Objective

The drone trajectory planning objective in the framework shown in Figure 1 is based on minimizing the anticipated variance on state and parameter estimates. In other words, we aim to identify the set of information maximizing observations among the possible observations that can be collected along a set of candidate trajectories. Navigating the drone to minimize the expected variance of the error on the state or parameter estimate is an instance of A-optimal control [34, 35, 36].

In particular, consider that $\hat{\psi}^{t+\Delta t}{}_{p}$ is the best traffic state or parameter estimate obtained after ΔT drone observations *into the future* along path p. The expected variance of the error on the state estimate is equivalent to the trace of the propagated error covariance matrix **P** as shown in Equation 19. We use this as a measure of future uncertainty $J^{t}{}_{p}{}^{+\Delta T}$ that results after the drone traverses path p. $J^{t}{}_{p}{}^{+\Delta T}$ can be computed separately for traffic states and incident parameters by propagating the state error covariance matrices using anticipated observations in the dual EnKF.

$$J_p^{t+\Delta T} = \mathbb{E}[||\psi_p^{t+\Delta T} - \hat{\psi}_p^{t+\Delta T}||_2^2] = \mathrm{tr}(\mathbb{E}[(\psi_p^{t+\Delta T} - \hat{\psi}_p^{t+\Delta T})(\psi_p^{t+\Delta T} - \hat{\psi}_p^{t+\Delta T})^T]) = \mathrm{tr}(\mathbf{P}) \tag{19}$$

However, to compare the relative uncertainty between traffic states and parameters, we need to normalize the magnitude of the involved variables. Specifically, the units chosen to represent densities and speed impact the resulting uncertainty measure $J^{t}{}_{p}{}^{+\Delta T}$ [36]. Since the dual EnKF maintains separate error covariance matrices, we are able to set the objective as a weighted sum of the trace matrices where the weights account for the differences in scale between densities and free flow speeds. Furthermore, the weights can be used to represent the importance of minimizing the uncertainty on parameters relative to traffic states. We also normalize for the number of traffic state variables in the densities EnKF, K, and the number of parameters in the free flow speeds EnKF,V, to ensure that the resulting uncertainty measures are comparable.

Thus, if we denote $J^{t+\Delta t}{}_{p,vmax}$ as the trace of the free flow speeds state error covariance matrix after ΔT observations along path p , $J^{t+\Delta t}{}_{p,\rho}$ to be the corresponding measure for traffic densities, and $\lambda \in [0,1]$ to be the weighting factor, we can formulate the future uncertainty measure $J^{t}{}_{p}{}^{+\Delta T}$ over possible drone paths as shown in Equation 20. Then, we aim to determine the path p^{*} that minimizes this uncertainty measure among the set of m candidate trajectories $\{p_1, \dots, p_m\}$ as shown in Equation 21.

$$J_p^{t+\Delta T} = \frac{\lambda}{V} J_{p,v_{max}}^{t+\Delta T} + \frac{(1-\lambda)}{K} J_{p,\rho}^{t+\Delta T} \tag{20}$$

$$p^* = \mathrm{argmin}_{p_1,..,p_m} J_p^{t+\Delta T} \tag{21}$$

Note that to compute $\hat{\psi}^{t+\Delta t}{}_{p}$ and $J^{t}{}_{p}{}^{+\Delta T}$ (uncertainty propagation and quantification), we need to embed an EnKF that propagates ensemble members at the current time t into the future $t + \Delta T$ using anticipated drone density observations along path p. Therefore, the framework in Figure 1 is composed of (1) a global dual state EnKF that updates state error covariance matrices at every time step using actual drone and ground sensor measurements, and (2) multiple dual state EnKFs that are initiated at every time step to propagate current ensemble members into the future based on anticipated drone measurements along each path. This allows us to determine the reduction in uncertainty along each candidate path and the path p^* that minimizes future uncertainty.

Furthermore, to compute $J^{t}{}_{p}{}^{+\Delta T}$, we need to define the anticipated drone observations along candidate paths. We can determine the drone location at every time step in ΔT using the drone speed and its direction of movement along a path. We also assume that the drone can observe a specified length of the road underneath its location. Then, for every drone location and time step in ΔT, we consider that the density observations at the drone location will be equal to the mean of density ensembles propagated by the forward model. In other words, the cell transmission model $\text{CTM}_{\Delta t}$ is used to propagate the density ensembles at time t up to the desired time step, and the mean of the propagated ensembles is considered to be the future density measurements. As for the free flow speed parameters, we consider that the drone can directly observe the true values up to observation errors once it reaches an incident prone segment. This implies that the future traffic state uncertainty measure relies on the variance of the current covariance matrices and the reduction in this variance due to anticipated drone observations. On the other hand, the future free flow speeds uncertainty measure corresponds to the drone observation errors.

Online Approximation and Optimization

Once the drone moves along the variance minimizing path p^* as determined by the trajectory planning objective in Equations 19-21, it feeds accurate density measurements and direct v_{max} observations to the global dual state EnKF. Then, the global dual state EnKF updates the state error covariance matrices and $\text{CTM}_{\Delta t}$ parameters based on observations from all available sensors (loop detectors, probe vehicles, and drone measurements). Since the network information is continuously updated, the resulting anticipated future uncertainty measure $J^{t}{}_{p}{}^{+\Delta T}$ dynamically changes. Specifically, to calculate $J^{t}{}_{p}{}^{+\Delta T}$, the state error covariance matrix after ΔT time steps should be obtained by propagating the current error statistics into the future along candidate paths using the embedded EnKFs and anticipated drone observations. Therefore, $J^{t}{}_{p}{}^{+\Delta T}$ must be re-calculated using the updated state error covariance matrices, drone position, and traffic model.

To control the drone in this online setting and reduce the number of candidate trajectories that should be evaluated, we use a one-step lookahead policy where at each time step we move the drone in the direction of the path that minimizes an approximation of the uncertainty measure [37]. The approximate uncertainty measure, $\tilde{J}^{t}{}_{p}{}^{+\Delta T}$, is based on the assumption that if a drone follows a particular path it would remain moving in the same direction along that path for the entire duration ΔT. In other words, we disregard the possibility of hovering or backtracking. After moving the

drone for one time step, we recompute the direction that minimizes $\tilde{J}^{t}{}_{p}{}^{+\Delta T}$ using the updated network information and drone location. The entire procedure is shown in Algorithm 2.

Algorithm 2 On-line algorithm for drone routing and estimation using the dual EnKF

Initialization:

(1) Define $\mathrm{CTM}_{\Delta t}$ based on incident free calibrated parameters
(2) Create initial ensembles for densities across cells
(3) Create initial ensembles for free flow speeds at incident prone locations
(4) Set initial drone location

Dual EnKF & drone routing:

for *time* in *estimation horizon* **do**
(4) Propagate density ensembles forward using Equations 3–6
(5) Update density ensembles using the global dual state EnKF through Equations 7–14 (include drone observations)
if get speed observation **or** drone at incident prone location **then**
(6) Propagate free flow speeds ensembles using Equation 15
(7) Use mean of densities ensemble, Equations 2, 7–12, and 14–18 to update free flow speeds ensembles using the global dual state EnKF (include drone observations)
(8) Update v_{max} and ρ_{cr} parameters in $\mathrm{CTM}_{\Delta t}$ using mean of free flow speeds ensembles and Equation 18
(9) Generate possible drone paths from current location
(10) For ΔT time steps, determine drone location at every time step along each path
(11) Generate predicted future drone density observations by propagating current density ensembles forward using $\mathrm{CTM}_{\Delta t}$ along each path
(12) Assuming drone will observe simulated density observations and actual free flow speeds at incident prone locations, use embedded dual state EnKF for ΔT steps into the future to determine $J_{p}^{t+\Delta T}$ along each candidate path
(13) Move drone one step in direction of p^* (the path with minimum $J_{p}^{t+\Delta T}$)

Chapter 4. Results and Conclusions

4.1 Results

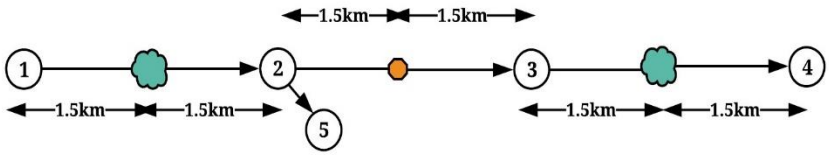

Figure 4 VISSIM test network.

As a proof of concept, we implement in this section the proposed algorithms (Algorithm 1 in Section 3 and Algorithm 2 in Section 4) on a freeway with an off-ramp modeled in VISSIM [27]. The freeway length, drone starting position, and incident prone locations are shown in Figure 4. In this figure, clouds indicate incident locations and the middle circle indicates the drone starting position.

In VISSIM, non-recurrent congestion at incident prone location is modeled using a reduced speed zone where the maximum speed is set in the range of 20 km/hr. The inflow demand at node 1 in Figure 4 is set at 6,600 veh/hr. At node 2, half of the demand continues on to node 4 while the other half takes the off-ramp. We use these model parameters to simulate congested conditions upstream (region B in Figure 3) and uncongested conditions downstream (region A in Figure 3). In terms of observations, we consider that loop detectors feed density measurements at every time step (10 seconds), and that speed measurements are collected from GPS equipped probe vehicles every 30 time steps (5 minutes).

For Algorithm 2, we set λ = 0.5 to represent equal weights for traffic state and parameter uncertainty measures. We determine ΔT dynamically as the number of time steps until the drone reaches node 1 if it is traveling upstream, or the number of time steps until it reaches node 4 if it is traveling downstream. We assume that the drone can observe 250 meters at every time step. We consider that the dual EnKF parameters are as follows: $w \sim N(0,25)$, $\varepsilon_j \sim N(0,25)$, $z \sim N(0,100)$, N = 100. The initial calibrated parameters were: ρ_{cr}^{0} =80veh/km, v_{max}^{0} = 100km/hr, ρ_j = 300veh/km.

Algorithms 1 and 2 were both able to accurately estimate densities along the freeway. As shown in Figure 5, the upstream density at the incident prone location was estimated to be around 200 veh/km. The downstream density estimates at the incident location varied significantly during the estimation time horizon as shown in Figure 6. In these figures, the solid lines indicate true density data from VISSIM, the dotted lines indicate the dual EnKF estimates (Algorithm 1), and the dashed lines indicate UAV-EnKF estimates (Algorithm 2).

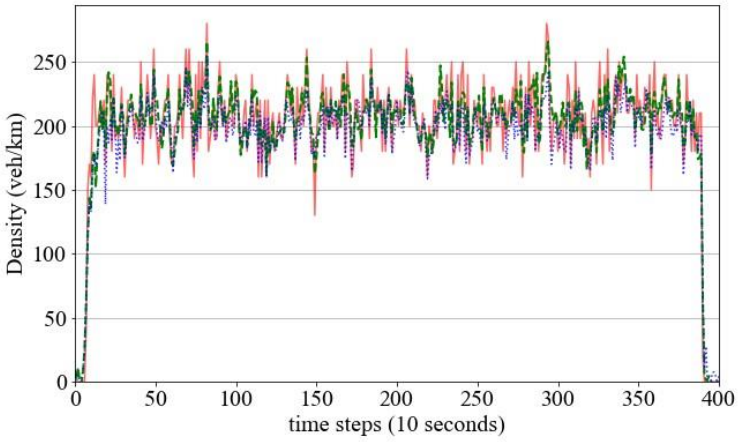

Figure 5 Estimated density at the upstream incident location (congested).

In terms of free flow speed estimation, the performance of Algorithm 1 differs significantly between uncongested and congested conditions. Specifically, as shown in Figure 8, in uncongested conditions the dashed line corresponding to Algorithm 1 quickly converges to the true free flow speed at 20 km/hr. However, as shown in Figure 7 corresponding to congested conditions at the upstream incident location, Algorithm 1 is not able to identify the true free flow speed since it is operating in region B of Figure 3. In these figures, the dashed horizontal line at 20km/hr indicates ground truth, dashed lines indicate dual EnKF estimates, and solid line indicates UAV-EnKF estimates.

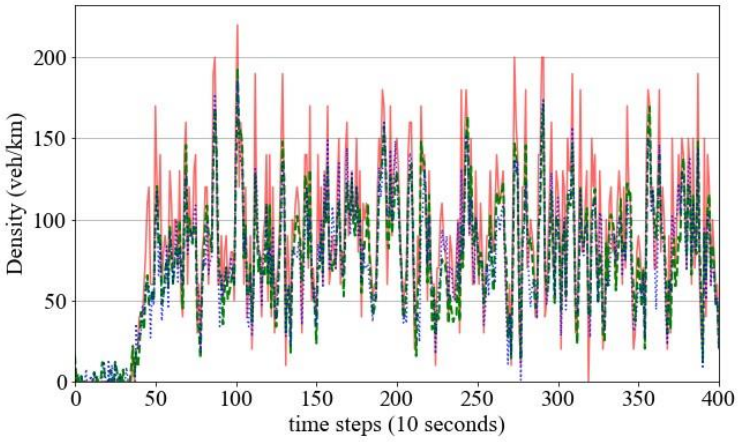

Figure 6 Estimated density at the downstream incident location (uncongested).

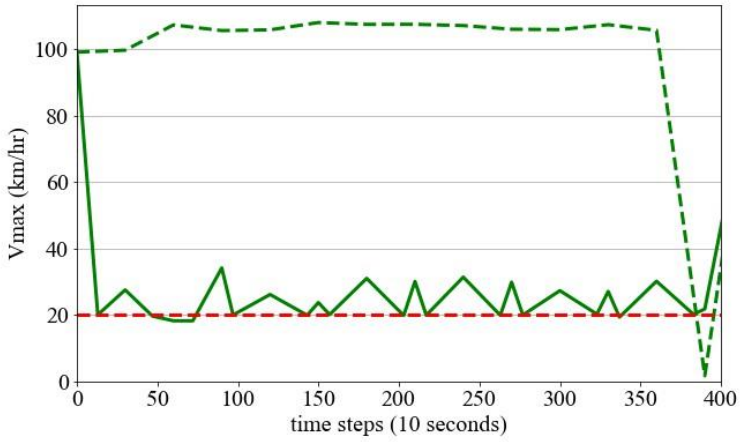

Figure 7 Estimated free flow speed at the upstream incident location (congested).

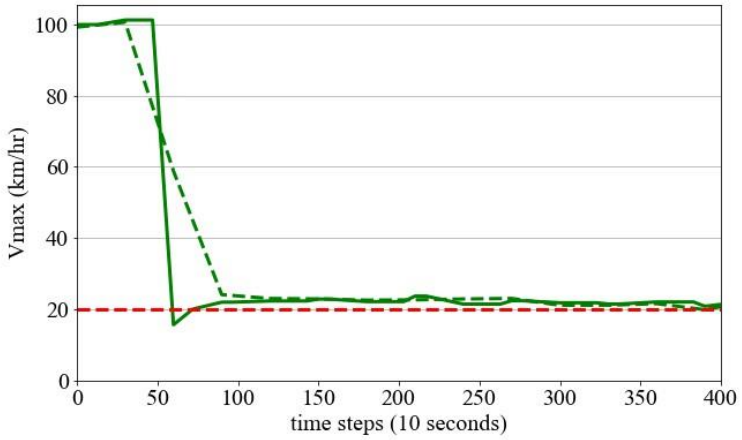

Figure 8 Estimated free flow speed at the downstream incident location (uncongested).

When a drone is introduced to aid in the estimation process, we can observe that the estimates of Algorithm 2 in Figure 7 (solid line) quickly converges to the true value of the free flow speed. This is a result of the targeted v_{max} observations collected by the drone. In particular, since the upstream incident prone location is congested, the initial v_{max} estimates at that location will have a high variance. This variance prompts the drone to navigate in the upstream direction (path from center to node 1). Once the drone arrives at the upstream location, it directly determines v_{max} up to observation errors.

We can observe from Figures 7 and 8 that the UAV-EnKF parameter estimates in uncongested conditions are smoother than the corresponding estimates in congested conditions. This reflects the high variance in congested conditions. Specifically, in congested conditions, a

wide range of free flow speeds may generate the speed and density measurements obtained from ground sensors. Therefore, even after the drone determines that the free flow speed is in the range of 20km/hr, subsequent ground sensor measurements are not informative and will result in noisy estimates reflecting the range of possible v_{max} values. However, in uncongested conditions, ground sensors and drone observations agree that v_{max} is in the range of 20km/hr (up to observation errors) which results in smooth estimates.

To investigate the planning process resulting from Algorithm 2, we plot the drone movement on the freeway across time in Figure 9. We can observe that the drone first moves to the upstream incident location since the variance on the upstream free flow speed is higher than the corresponding downstream variance. Once the drone observes the true conditions at the upstream incident location, it reverses direction towards the downstream incident. However, since the v_{max} parameters are propagated through a random walk and the congested conditions at the upstream incident limit the ability to identify the true parameter, the drone decides to go back to the upstream incident location before it reaches the downstream incident. This is expected since as shown in Figure 8 the dual EnKF without drone can effectively estimate the true parameter at the uncongested downstream location.

After obtaining 2 observations at the congested upstream location, the drone moves to the downstream incident and continues to traverse the freeway as shown in Figure 9. We note that the drone spends 62% of the total estimation time between the middle starting position and the upstream incident prone location. This further shows the need for drone observations in congested conditions that correspond to region B of Figure 3.

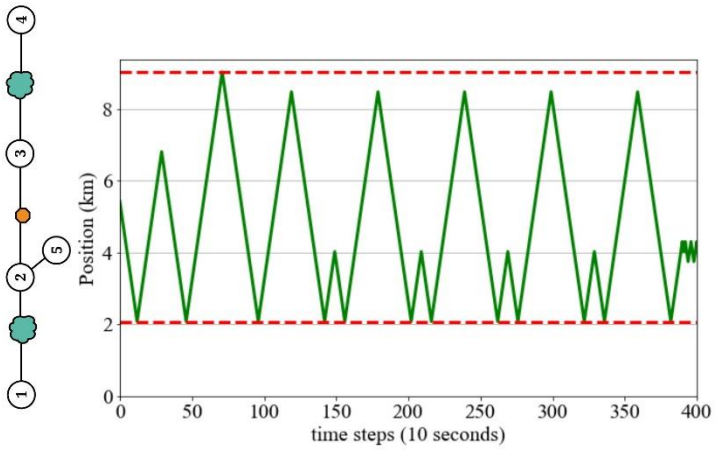

Figure 9 Drone movement across time. Dashed lines indicate incident locations.

4.2 Conclusions

Non-recurrent congestion is a primary source of travel time variability and congestion delays. Traditional data-driven methods for detecting non-recurrent congestion are not capable of simultaneously estimating traffic and road network conditions. In addition, these data-driven

methods are susceptible to false alarms. On the other hand, model-based methods that simultaneously estimate traffic conditions and incident severity suffer in congested conditions where it is difficult to distinguish between observations from congestion under normal operating conditions and similar observations that result due to reductions in capacity.

We propose a coupled planning and estimation framework that relies on unmanned aerial vehicles (drones) to generate targeted observations which minimize a weighted uncertainty on incident parameters and traffic states. Specifically, we develop an on-line one step lookahead algorithm that uses a dual ensemble Kalman filter (EnKF) to determine the uncertainty minimizing drone path at every time step. We test the algorithm on a freeway network and compare its performance against a dual EnKF that is not aided by drone observations. The drone assisted dual EnKF shows significant improvement in estimation capabilities under congested conditions. In particular, the drone observations allow us to determine the exact road condition up to observation error when this is not possible otherwise.

4.3 Directions for Future Research

In future work, we aim to seek alternative methods for quantifying and minimizing uncertainty over larger networks. Further, we aim to investigate parcel delivery algorithms that rely on the capability of drones to extract road and traffic information. In particular, the proposed framework determines which drone observations are informative and navigates the drone to minimize uncertainty. However, when the drone is required to deliver parcels as it operates in tandem with a truck, there are additional constraints and decision controls that pertain to visiting customers. Thus, while the truck benefits from the drone traffic observations in determining paths that reduce its travel time, there are additional factors that we need to consider when routing the drone and deploying it to deliver parcels.

References

[1] A. Skabardonis, P. Varaiya, and K. Petty. Measuring recurrent and nonrecurrent traffic congestion. *Transportation Research Record: Journal of the Transportation Research Board*, 1856, 2003.

[2] B. Anbaroglu, B. Heydecker, and T. Cheng. Spatio-temporal clustering for non-recurrent traffic congestion detection on urban road networks. *Transportation Research Part C: Emerging Technologies*, 48, 2014.

[3] Y. J. Stephanedes and A. P. Chassiakos. Freeway incident detection through filtering. *Transportation Research Part C: Emerging Technologies*, 1(3), 1993.

[4] R. L. Cheu and S. G. Ritchie. Automated detection of lane-blocking freeway incidents using artificial neural networks. *Transportation Research Part C: Emerging Technologies*, 3(6), 1995.

[5] R. Wang, D. B. Work, and R. Sowers. Multiple model particle filter for traffic estimation and incident detection. *IEEE Transactions on Intelligent Transportation Systems*, 17(12), 2016.

[6] A. Dabiri and B. Kulcsár. Freeway traffic incident reconstruction – a biparameter approach. *Transportation Research Part C: Emerging Technologies*, 58, 2015.

[7] Y. Wang and M. Papageorgiou. Real-time freeway traffic state estimation based on extended Kalman filter: A general approach. *Transportation Research Part B: Methodological*, 39(2), 2005.

[8] A. Willsky, E. Chow, S. Gershwin, C. Greene, P. Houpt, and A. Kurkjian. Dynamic model-based techniques for the detection of incidents on freeways. *IEEE Transactions on Automatic Control*, 25(3), 1980.

[9] R. Wang and D. B. Work. Interactive multiple model ensemble Kalman filter for traffic estimation and incident detection. In *17th International IEEE Conference on Intelligent Transportation Systems (ITSC)*. IEEE, 2014.

[10] R. Wang, S. Fan, and D. B. Work. Efficient multiple model particle filtering for joint traffic state estimation and incident detection. *Transportation Research Part C: Emerging Technologies*, 71, 2016.

[11] Y. Wang, M. Papageorgiou, M. Messmer, P. Coppola, A. Tzimitsi, and A. Nuzzolo. An adaptive freeway traffic state estimator. *Automatica*, 45 (1), 2009.

[12] K. K. Sanwal, K. Petty, J. Walrand, and Y. Fawaz. An extended macroscopic model for traffic flow. *Transportation Research Part B: Methodological*, 30 (1), 1996.

[13] H. J. Payne and S. C. Tignor. Freeway incident-detection algorithms based on decision trees with states. *Transportation Research Record*, 1978.

[14] H. Teng and Y. Qi. Application of wavelet technique to freeway incident detection. *Transportation Research Part C: Emerging Technologies*, 11, 2003.

[15] H. Dia and G. Rose. Development and evaluation of neural network freeway incident detection models using field data. *Transportation Research Part C: Emerging Technologies*, 5(5), 1997.

[16] Y. J. Stephanedes and X. Liu. Artificial neural networks for freeway incident detection. *Transportation Research Record*, 1995.

[17] Y. J. Stephanedes, A. P. Chassiakos, and P. G. Michalopoulos. Comparative performance evaluation of incident detection algorithms. *Transportation Research Record*, 1360, 1992.

[18] E. Parkany and C. Xie. A review of incident detection technologies, algorithms and their deployments: What works and what doesn't. Technical Report NETCR37, University of Massachusetts Transportation Center, 2005.

[19] Z. Sun, W. Jin, and S. G. Ritchie. Simultaneous estimation of states and parameters in Newell's simplified kinematic wave model with Eulerian and Lagrangian traffic data. *Transportation Research Part B: Methodological*, 104, 2017.

[20] J. Y. J. Chow. Dynamic UAV-based traffic monitoring under uncertainty as a stochastic arc-inventory routing policy. *International Journal of Transportation Science and Technology*, 5(3), 2016.

[21] H. Ikeda, Y. Kaneko, T. Matsuo, and K. Tsuji. Abnormal incident detection system employing image processing technology. In *Proceedings 199 IEEE/IEEJ/JSAI International Conference on Intelligent Transportation Systems*, 1999.

[22] K. Wang, X. Jia, and S. Tang. A survey of vision-based automatic incident detection technology. In *IEEE International Conference on Vehicular Electronics and Safety, 2005*, 2005.

[23] E. S. Canepa and C. G. Claudel. Networked traffic state estimation involving mixed fixed-mobile sensor data using Hamilton-Jacobi equations. *Transportation Research Part B: Methodological*, 104, 2017.

[24] C. F. Daganzo. The cell transmission model: A dynamic representation of highway traffic consistent with the hydrodynamic theory. *Transportation Research Part B: Methodological*, 28(4), 1994.

[25] C. F. Daganzo. The cell transmission model, Part II: Network traffic. *Transportation Research Part B: Methodological*, 29(2), 1995.

[26] S. Godunov. A difference method for the numerical calculation of discontinuous solutions of hydrodynamic equations. *Mathematics Sbornik*, 47(3), 1959.

[27] P. T. V. Group. PTV Vissim. http://vision-traffic.ptvgroup. com/en-us/products/ptv-vissim/, 2018.

[28] G. Evensen. The ensemble Kalman filter: Theoretical formulation and practical implementation. *Ocean Dynamics*, 53(4), 2003.

[29] G. Evensen. *Data Assimilation: The Ensemble Kalman Filter*. Springer Science & Business Media, 2009.

[30] S. Blandin, A. Couque, A. Bayen, and D. Work. On sequential data assimilation for scalar macroscopic traffic flow models. *Physica D: Nonlinear Phenomena*, 241(17), 2012.

[31] S. Haykin. *Kalman Filtering and Neural Networks*, volume 47. John Wiley & Sons, 2004.

[32] J. W. C. Van Lint, S. P. Hoogendoorn, and A. Hegyi. Dual EKF state and parameter estimation in multi-class first-order traffic flow models. In *IFAC Proceedings Volumes*, volume 41, 2008.

[33] A. Hegyi, D. Girimonte, R. Babuska, and B. De Schutter. A comparison of filter configurations for freeway traffic state estimation. In *Intelligent Transportation Systems Conference, 2006. ITSC'06*. IEEE, 2006.

[34] D. Ucinski. *Optimal Measurement Methods for Distributed Parameter System Identification*. CRC Press, 2004.

[35] A. Atkinson, A. Donev, and R. Tobias. *Optimum Experimental Designs, with SAS*, volume 34. Oxford University Press, 2007.

[36] R. Sim and N. Roy. Global A-optimal robot exploration in SLAM. In *Proceedings of the 2005 IEEE International Conference on Robotics and Automatio*. IEEE, 2005.

[37] D. P. Bertsekas. *Dynamic Programming and Optimal Control*, volume 1. Athena Scientific, 4th edition, 2017.